

1 **OrBITS: A High-throughput, time-lapse, and label-free drug screening platform for patient-**
2 **derived 3D organoids**

3
4 **Authors:** Christophe Deben^{1*}, Edgar Cardenas De La Hoz^{2*}, Maxim Le Compte¹, Paul Van
5 Schil³, Jeroen M. Hendriks³, Patrick Lauwers³, Suresh Krishan Yogeswaran³, Filip Lardon¹,
6 Patrick Pauwels^{1,4}, Annemie Bogaerts⁶, Evelien Smits^{1,5}, Steve Vanlanduit², Abraham Lin^{1,6}

7 *Both authors contributed equally to the manuscript. Christophe Deben for the biological part, Edgar Cardenas De La Hoz for the computational
8 part.

- 9 1. Center for Oncological Research (CORE), Integrated Personalized & Precision Oncology Network (IPPON), University of Antwerp, Wilrijk,
10 Belgium.
11 2. Industrial Vision Lab, University of Antwerp, Groenenborgerlaan 171, Antwerp 2020, Belgium
12 3. Department of Thoracic and Vascular surgery, Antwerp University Hospital, Edegem, Belgium.
13 4. Department of Pathology, Antwerp University Hospital, Edegem, Belgium.
14 5. Center for Cell Therapy and Regenerative Medicine, Antwerp University Hospital, Edegem, Belgium.
15 6. Plasma Lab for Applications in Sustainability and Medicine ANTwerp (PLASMANT), University of Antwerp, 2610 Wilrijk, Belgium.
16
17
18
19
20
21

22

23

24

25 **Abstract**

26 Patient-derived organoids are invaluable for fundamental and translational cancer research and
27 holds great promise for personalized medicine. However, the shortage of available analysis
28 methods, which are often single-time point, severely impede the potential and routine use of
29 organoids for basic research, clinical practise, and pharmaceutical and industrial applications.
30 Here, we report the development of a high-throughput automated organoid analysis platform that
31 allows for kinetic monitoring of organoids, named **Organoid Brightfield Identification-based**
32 **Therapy Screening (OrBITS)**. The combination of computer vision with a convolutional network
33 machine learning approach allowed for the detection and tracking of organoids in routine
34 extracellular matrix domes, advanced Gri3D[®]-96 well plates, and high-throughput 384-well
35 microplates, solely based on brightfield imaging. We used OrBITS to screen chemotherapeutics
36 and targeted therapies, and incorporation of a fluorescent cell death marker, revealed further
37 insight into the mechanistic action of the drug, a feature not achievable with the current gold
38 standard ATP-assay. This manuscript describes the validation of the OrBITS deep learning
39 analysis approach against current standard assays for kinetic imaging and automated analysis of
40 organoids. OrBITS, as a scalable, high-throughput technology, would facilitate the use of patient-
41 derived organoids for drug development, therapy screening, and guided clinical decisions for
42 personalized medicine. The developed platform also provides a launching point for further
43 brightfield-based assay development to be used for fundamental research.

44

45

46

47 **Introduction**

48 The use of 2D cancer cell lines has traditionally been the gold standard in preclinical *in vitro* cancer
49 research. However, these models fail to recreate the complex cell-cell interactions present in the
50 tumor microenvironment and lack the genetic heterogeneity found in cancer patients. In addition,
51 prolonged use of these cancer cell lines lead to acquired mutations or gene expression alterations,
52 which are often overlooked as the cell line deviates from the originally derived tumor. As a result,
53 new therapies are often met with high failure rates during translation from preclinical research to
54 clinical trials, thus resulting in extreme forfeiture of research labor and financial loss.

55 The development of 3D cell culture technologies has greatly improved the physiological relevance
56 of *in vitro* cancer models and the use of patient-derived organoids (PDOs) is revolutionizing basic
57 and translation cancer research ¹. These PDOs resemble both the pheno- and genotype of the tissue
58 they are derived from and can be expanded long-term and cryopreserved to establish a living tumor
59 and healthy tissue biobank ¹. Furthermore, one of the most promising applications of PDOs is for
60 personalized cancer treatment to predict clinical response *ex vivo* ²⁻⁸. However, the available
61 repertoire of assays for high-throughput organoid analysis is severely limited, and therefore, the
62 current gold standard relies on a rudimentary viability assay.

63 The gold standard analysis method, Promega CellTiter-Glo 3D cell viability assay, determines the
64 number of viable cells in 3D cell cultures based on luminescent quantification of intracellular ATP
65 in both 96- and 384-well microplate format. This is method is met with several intrinsic limitations
66 including growth rate variations and (drug-induced) metabolic modulations, which could affect
67 the translatability of this readout. ⁹⁻¹¹ For drug screening and diagnostic applications, this assay is
68 also unable to determine the mechanistic action of the drug, such as cytostatic or cytotoxic

69 response, and is limited to a single time-point analysis. These aspects critically limit the wide
70 adoption of organoid technology for clinical diagnostics and pharmaceutical drug screening.
71 Therefore, although the CellTiter-Glo viability assay has been a valuable method to monitor drug
72 responses, more sophisticated high-throughput analysis methods are urgently needed.
73 In this study, we addressed these shortcomings by using an automated, high-throughput, and
74 kinetic screening platform to monitor therapy response. Using the Tecan Spark Cyto multi-mode
75 plate reader system, we automated seeding of full-grown PDOs in a 384-well format and
76 performed real-time, whole-well brightfield (BF) and fluorescence imaging in a temperature, CO₂,
77 and O₂ controlled environment. This reduces the variability involved in manual organoid cultures,
78 which is highly cumbersome and not scalable. Using software, which utilizes convolutional
79 network machine learning to eliminate the use of fluorescent viability markers, we validated the
80 capacity for BF imaging-based monitoring of PDO growth and viability, by comparing our results
81 to the current industry and research standards. The combination of BF imaging with a fluorescent
82 cell death marker further demarcated cytostatic from cytotoxic therapy responses, thus providing
83 greater insight into drug effects and the potential for improving translation into a durable clinical
84 response in patients. The combination of the automated seeding and image-based monitoring of
85 PDOs constitutes our novel integrated platform OrBITS (**O**rganoid **B**rightfield **I**dentification-
86 based **T**herapy **S**creening). Using OrBITS, we performed a screening of several chemotherapeutics
87 and targeted therapies on patient-derived organoids as a proof-of-concept. The technology
88 described here to produce and validate our drug screening platform unlocks the potential for wide
89 adoption of organoid-based assays for drug screening and discovery as well as guidance of clinical
90 decision for personalized medicine.

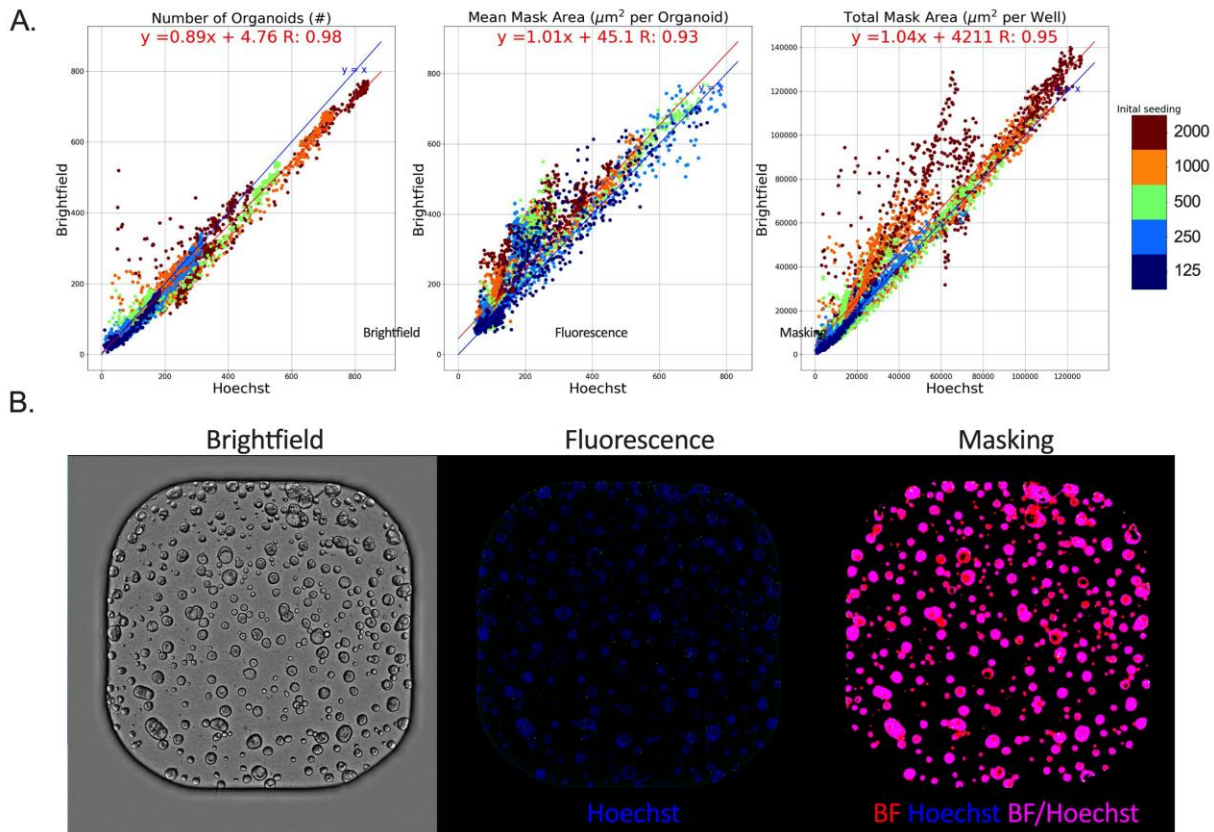
91 **Results**

92 *Patient-derived lung organoids*

93 Validation of the organoid monitoring ability using BF imaging was performed on various lung
94 organoid lines. Organoids derived from patient tumor resection fragments had a predominantly
95 solid growth pattern, while organoids derived from distant healthy lung tissue displayed a cystic
96 growth pattern (Fig. S1). Further characterization of the tumor tissue-derived organoids indicated
97 that the cells were non-malignant and most likely represent metaplastic squamous epithelial cells
98 (details in supplementary information)^{12,13}. These observations confirmed the challenges related
99 to generating pure lung tumor organoids as first described by Dijkstra and colleagues.¹³ However,
100 for validation of organoid monitoring with OrBITS, these non-malignant organoids were equally
101 relevant. The cystic NSCLC_006N and NSCLC_051N organoids and solid NSCLC_013T,
102 NSCLC_046T and NSCLC_051T organoids were used in the subsequent experiments.

103 *Validation of label-free Brightfield monitoring of all stages of organoid growth*

104 A kinetic image set was generated from a serial dilution of single cells and 3-day old organoids
105 grown in a 384-well microplate from two organoid lines (NSCLC_013T and NSCLC_006N)
106 stained with Hoechst as a gold standard reference method. Pairwise comparison showed a strong
107 correlation of the organoid Count, Mean Area, and Total Area detected by BF when compared to
108 Hoechst for the entire range of sizes (Fig. 1A). This indicates that OrBITS is capable of kinetic
109 monitoring at all stages of organoid growth in the absence of a fluorescent dye and based solely
110 on BF image analysis (Fig. 1B, Supplemental Video 1-3).



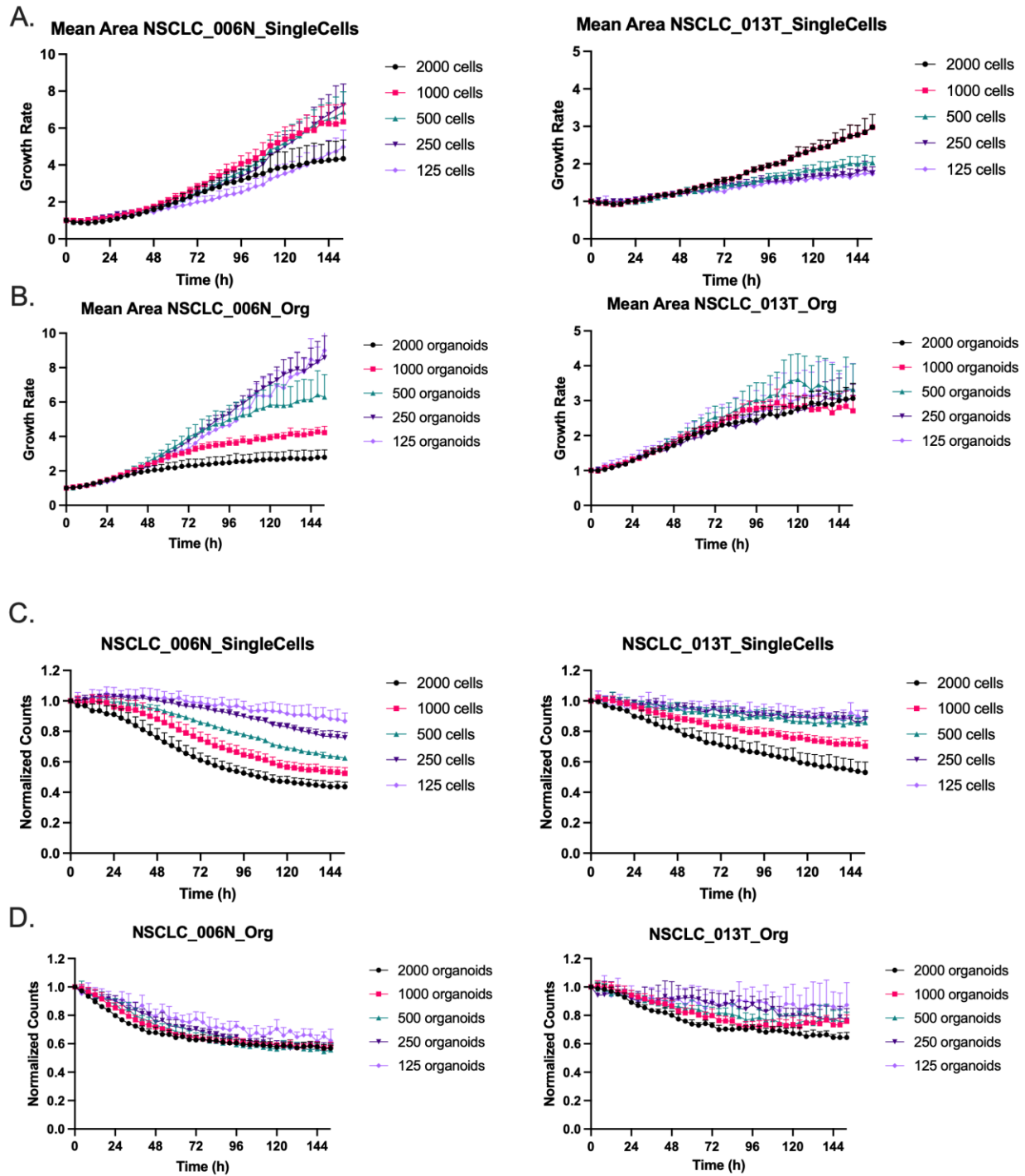
111

112 **Figure 1: Brightfield versus Hoechst.** (A) Pairwise comparison of organoid Counts, Mean Mask
113 Area and Total Mask Area detected by Brightfield- and Hoechst-based analysis of NSCLC_013T
114 and NSCLC_006N PDO lines plated as a serial dilution of single cells and 3-day old organoids
115 (Table S2). (B) Representative whole 384-well brightfield and fluorescent images of full-grown
116 PDOs and the corresponding analysis mask. Supplemental Video 3 presents the corresponding
117 time-laps video.

118

119 Both organoid lines could be grown from either single cells (Fig. 2A) or fully-grown organoids,
120 which are more conventionally used (Fig. 2B). An important advantage of the proposed assay is
121 that growth kinetics can be accurately monitored using only a limited amount of starting material.
122 In fact, using a larger number of single cells or organoids affected BF image monitoring results in
123 two ways: (i) when both lines (NSCLC_013T and NSCLC_006N) were plated at high single cell
124 densities, a drop in counts was observed over time due to organoids merging or fusion events (Fig.

125 2C-D, Supplemental Video 1) resulting in an aberrant growth rate based on Mean Area for
126 NSCLC_013T at higher seeding densities (Fig. 2A); (ii) NSCLC_006N PDOs showed a higher
127 growth rate compared to NSCLC_013T PDOs due to differential nutrient requirements. At higher
128 concentrations (>500 counts), we clearly observed a drop in NSCLC_006N organoids growth rate
129 compared to the slower growing NSCLC_013T organoids due to the lack of nutrients (Fig. 2B).



130

131 **Figure 2: Influence of seeding density.** Average growth rate of PDOs seeded as (A) single cells or (B) 3-day old
132 organoids. Normalized counts (h=0) of PDOs seeded as (C) single cells or (D) 3-day old organoids. A range between
133 125 – 2000 cells or organoids were plated. Graphs presented as mean \pm SD of 5 technical replicates and images were
134 acquired every 6 hours.

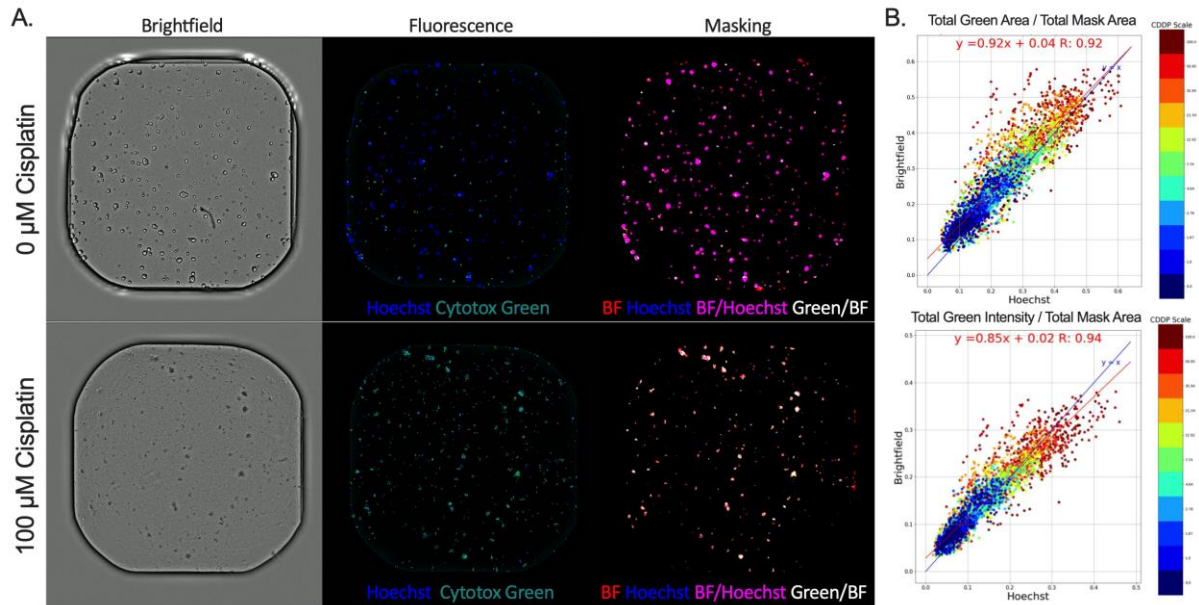
135 *Monitoring organoid death with intra-well normalization*

136 Since PDOs used in drug screening will undergo varying degrees and stages of death, it is critical
137 that the OrBITS platform is able to detect such organoids. Therefore, a second kinetic image set
138 was generated from two organoid lines (NSCLC_051T and NSCLC_051N; 500/well plated as 2-
139 day old organoids) and treated with a 10-point titration of cisplatin. PDOs were stained with
140 Hoechst as the gold standard reference method and used for validation of BF image analysis.
141 Despite varying levels of cytotoxicity from the chemotherapeutic treatment, the data showed that
142 organoids were successfully identified from BF images (Fig. S2). Importantly, common artefacts
143 (e.g. air-bubbles, extracellular matrix, dust) did not disrupt BF analysis (Fig. S2).

144 To further develop the applicability of the OrBITS platform, we investigated the capacity for intra-
145 well normalization of organoid death with cell death markers, such as Cytotox Green. Since
146 Hoechst and Cytotox Green are both nuclear stains, the overlap of Green Area or Green Intensity
147 (RFU) with Hoechst allowed for intra-well normalization to study varying levels of cell death from
148 the chemotherapeutic treatment (Fig. 3A). Importantly, pairwise comparison showed a strong
149 correlation between BF and Hoechst normalized Green Area and Green Intensity, thus making a
150 fluorescent viability stain (nuclear or cytoplasmatic) redundant (Fig. 3B). Total Green Area / Total
151 Mask Area resulted in the broadest dynamic range ($\sim\Delta 0.6$ vs. $\sim\Delta 0.4$), although a complete overlap
152 ($R = 1$) in the 100 % cell death control (100 μ M CDDP) was not reached (Fig. 3B). Therefore, the
153 proposed platform provides an important advantage by including intra-well, normalized organoid
154 death, even without the use of a viability label.

155 Overall, we showed that our OrBITS platform can mask organoids with high accuracy ranging
156 from single cells to full-grown organoids based on BF imaging. In addition, inclusion of a

157 fluorescent cell death marker allowed for kinetic detection of intra-well normalized organoid
158 death. This allows for the removal of a nuclear or cytoplasmatic viability stain during kinetic
159 analysis, a key limitation of the current state-of-the-art analysis, as it can influence cellular growth
160 and health and confounds the effect of treatments.



161
162 **Figure 3: Brightfield vs Hoechst normalized fluorescent cell death marker.** (A) Representative brightfield and
163 fluorescent (Hoechst and Cytotox Green) images of untreated and 100 μM cisplatin (CDDP) treated NSCLC_051T
164 PDOs and the corresponding masking of Brightfield, Hoechst, Brightfield/Hoechst overlap and Cytotox
165 Green/Brightfield overlap. (B) Pairwise comparison of Total Green Area / Total Mask Area (per well: μm²/ μm²) and
166 Total Green Intensity / Total Mask Area (per well: RFU/ μm²) with Mask Area based on either Hoechst fluorescence
167 imaging or BF imaging (Table S2).

168
169 *Validation of OrBITS brightfield PDO monitoring in proof-of-concept drug screening:*

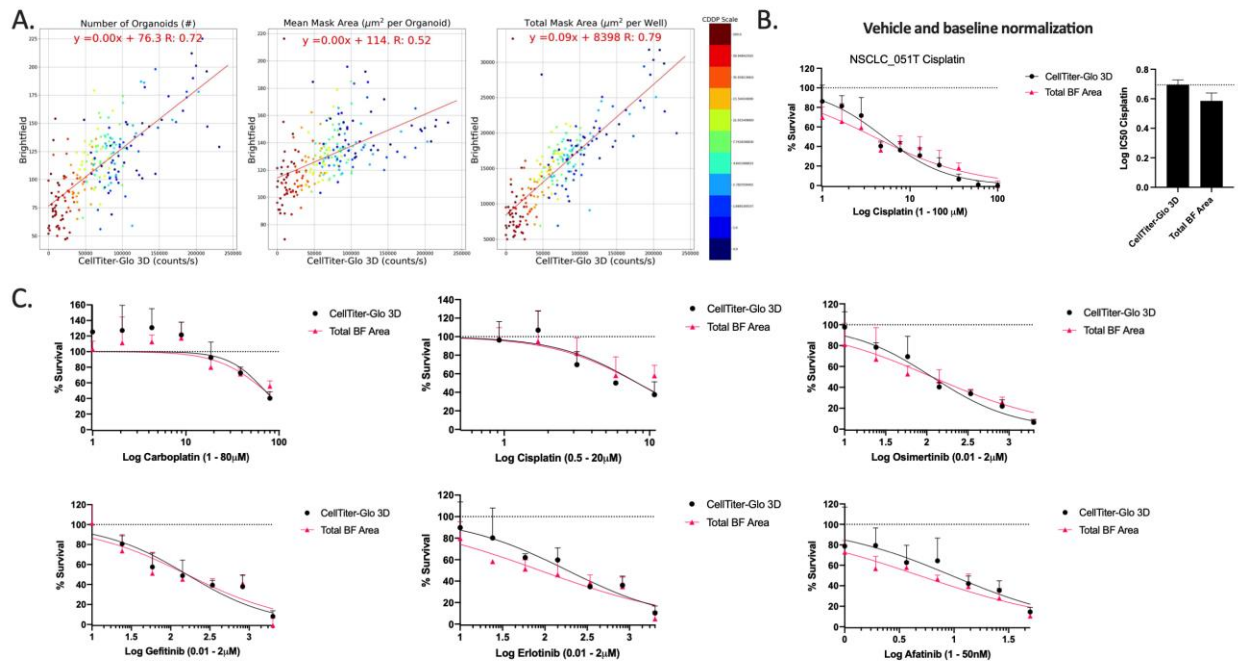
170 *Comparison to CellTiter-Glo3D*

171 In order to determine the if the OrBITS platform could accurately monitor viability and therapy
172 response in PDOs, we compared the BF image analysis with the current industry and research
173 standard: CellTiter-Glo 3D viability assay. PDOs were again treated with a 10-point titration of
174 cisplatin, analyzed with both the OrBITS platform and the CellTiter-Glo 3D viability assay, and

175 the read-outs were compared. Pairwise comparison revealed that the Total Mask Area had the
176 strongest correlation with the CellTiter-Glo 3D luminescent signal, since both parameters result
177 from whole-well readouts (Fig. 4A).

178 The assay quality was assessed based on the Z-factor, a coefficient reflective of both assay signal
179 dynamic range and data variation, using 100 μ M cisplatin as positive control for NSCLC_051T.
180 The CellTiter-Glo 3D read-out was characterized by a Z-factor of 0.78 and the Total BF Area by
181 a Z-factor of 0.69, indicating that the BF assay is excellent for drug screening. When applying both
182 vehicle (100% viability; PBS) and baseline normalization (0% viability; 100 μ M cisplatin) no
183 significant difference was observed between IC₅₀ values obtained by the Total BF Area analysis
184 and CellTiter-Glo 3D assay (Fig. 4B).

185 To validate our approach, we performed a drug screen of 6 standard-of-care lung cancer treatments
186 on an additional PDO line (NSCLC_013T) using 1 μ M staurosporine as the standardized 100%
187 cell death control. A clear overlap of the inhibitory dose-response curves (Fig. 4C) and
188 corresponding IC₅₀ values (Fig. S3) was observed between the Total Mask Area analysis and
189 CellTiter-Glo 3D assay. Therefore, it was clear that the OrBITS platform could accurately monitor
190 PDOs for various anti-cancer drug screenings.



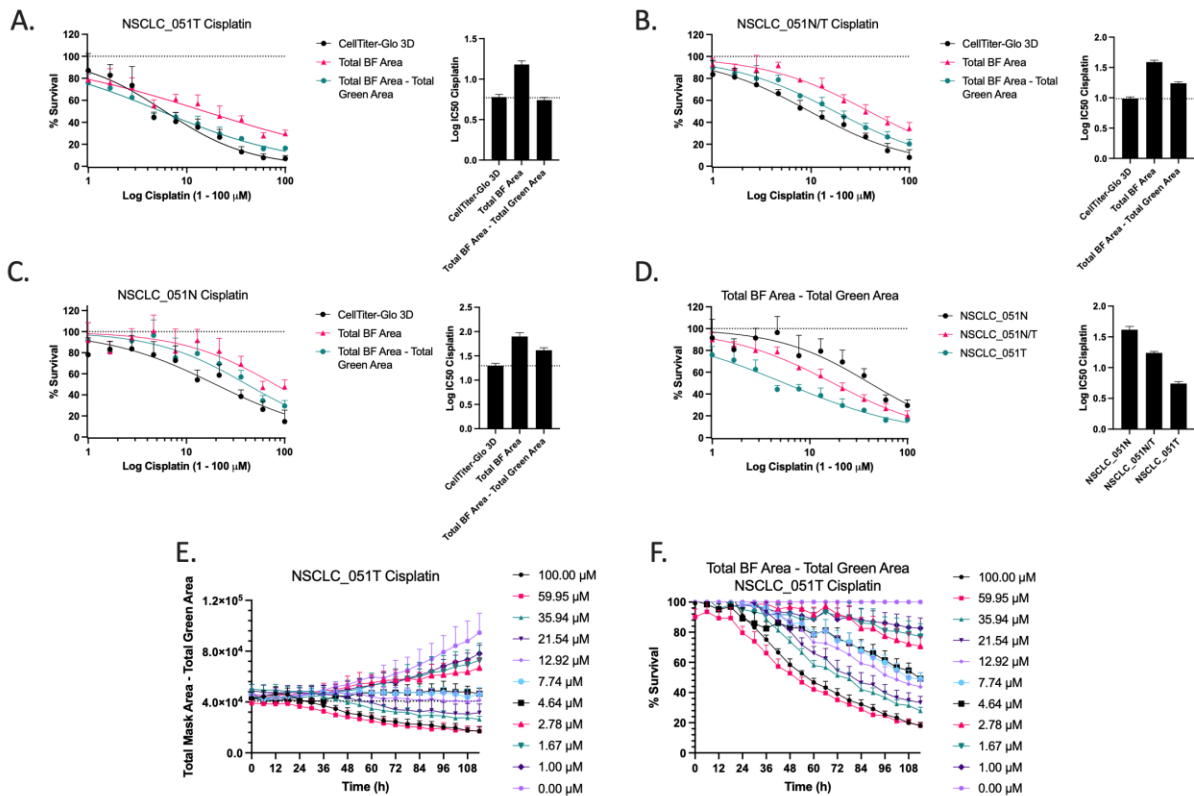
191

192 **Figure 4: Brightfield imaging as a viability marker to monitor therapy response.** (A) Pairwise comparison of
 193 organoid Count, Mean Mask Area and Total Mask Area with the luminescent read-out (counts/s) of the CellTiter-Glo
 194 3D assay for the NSCLC_051T, NSCLC_051N, co-culture NSCLC_051T/N and NSCLC_050N PDO lines treated
 195 with a 10-point titration of cisplatin. Both read-outs were acquired at the same timepoint (114 hours) (Table S2). (B)
 196 Dose-response curve and corresponding IC50-values for NSCLC_051T treated with a 10-point titration of cisplatin
 197 and normalized to vehicle (100%) and baseline (0%, 100 μM cisplatin). (C) Dose-response curves of NSCLC_013T
 198 PDOs treated with a 7-point titration of cisplatin, carboplatin, erlotinib, gefitinib, osimertinib or afatinib
 199 normalized to vehicle (100%) and baseline (0%, 1 μM staurosporine). Corresponding IC50 values are presented in fig. S3. Graphs
 200 presented as mean \pm SD of 5 technical replicates.

201

202 We observed that the Total BF Area resulted in an overestimation of the percentage of viable cells
 203 compared to the CellTiter-Glo 3D assay, following normalization to the vehicle control (Fig. 5A-
 204 C). The difference increased with cisplatin concentration, which was not unexpected since dead
 205 organoids were still counted by BF imaging. Therefore, we used a fluorescent cell death marker
 206 (Cytotox Green or equivalent) to correct for the area covered by dead entities, thus producing the
 207 parameter Total BF Area – Total Green Area. This parameter was characterized by a Z-factor of
 208 0.80 for the NSCLC_051T line and both the dose-response curves and IC50-values showed an
 209 improved overlap with the CellTiter-Glo 3D assay for NSCLC_051T, 051N/T and 051N organoids

210 (Fig. 5A-C). Importantly, the parameter showed a clear distinction in sensitivity between the
 211 NSCLC_051T and NSCLC_051N lines, with an intermediate response in the co-culture of both
 212 lines (Fig. 5D). In addition, this parameter allowed for kinetic monitoring of cell viability (Fig.
 213 5E) and vehicle-normalized survival (Fig. 5F), thus making early detection of therapy response
 214 possible.
 215 Overall, we demonstrated that the parameters used in our proposed BF image analysis were robust
 216 and determined cell viability and IC50-values corresponding to the gold standard CellTiter-Glo
 217 3D assay. Our OrBITS platform is a significant advance from the current gold standard assay by
 218 addressing its intrinsic limitations, as it allows for kinetic monitoring of organoid health and
 219 growth from limited starting material and independent of metabolic changes.



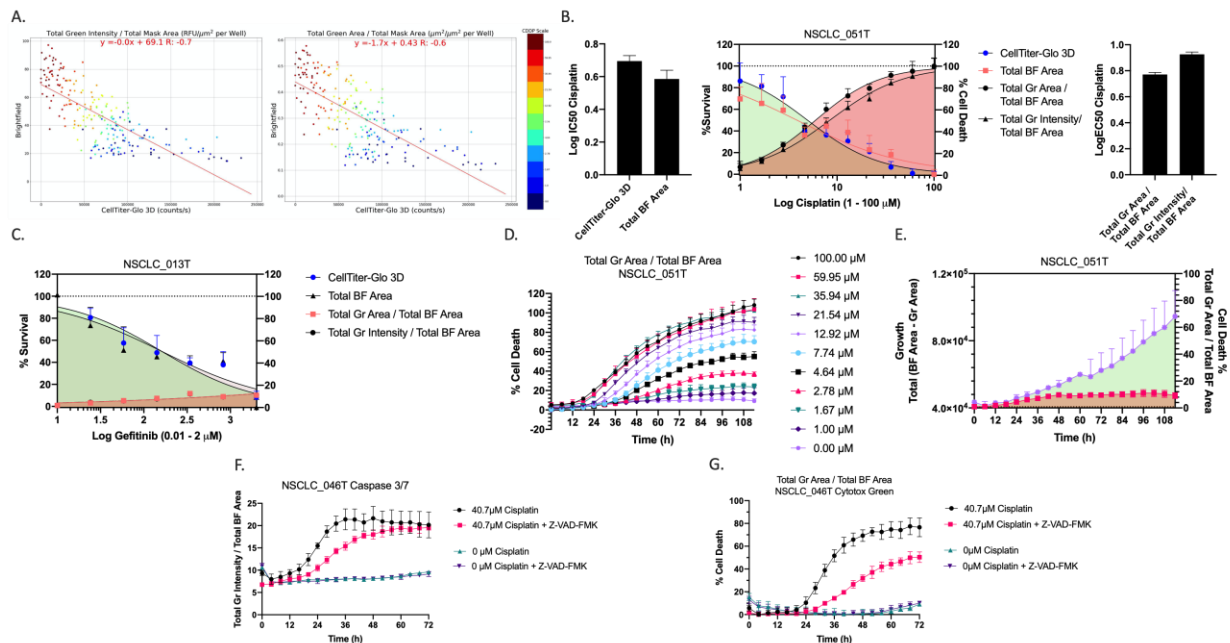
220

221 **Figure 5: Cell death corrected vehicle normalization.** (A-C) Dose-response curves and corresponding IC50-values
222 for NSCLC_051T, NSCLC_051N and co-culture NSCLC_051N/T treated with a 10-point titration of cisplatin and
223 normalized to vehicle (100%) control. Real-time monitoring of (E) cell viability and (F) survival percentage of
224 NSCLC_051T PDOs treated with a 10-point titration of cisplatin. Percent survival was baseline corrected to vehicle
225 control at each timepoint. Graphs presented as mean \pm SD of 5 technical replicates.
226

227 *Validation of OrBITS analysis to delineate cytostatic and cytotoxic anti-cancer therapy response*

228 The ATP-based PDO drug screening analysis method does not provide insight into the mechanistic
229 action of the drug, and therefore, we aimed to distinguish a cytostatic response (i.e. growth arrest)
230 from a cytotoxic response (i.e. cell death) using the OrBITS platform. To achieve this, we
231 quantified the amount of therapy-induced organoid death using our BF image analysis and the
232 CellTiter-Glo 3D assay. Pairwise comparison showed an inverse correlation of Total Green Area
233 and Total Green Intensity normalized to Total BF Area with the CellTiter-Glo 3D readout (Fig.
234 6A). The assay quality was assessed based on the Z-factor using 100 μ M cisplatin as positive
235 control for NSCLC_051T. Total Green Area / Total BF Area and Total Green Intensity / Total BF
236 Area were characterized by a Z-factor of 0.71 and 0.75, respectively, consistent with a robust assay.
237 A clear inverse relation was observed for the inhibitory dose-response curve (% survival) and
238 stimulatory dose-response curve of both the Total Green Area and Intensity parameters normalized
239 to BF area (% cell death) for cisplatin treated NSCLC_051T PDOs, suggesting a cytotoxic
240 response in this organoid line (Fig. 6B). An example of a cytostatic response is given for
241 NSCLC_013T treated with gefitinib (Fig. 6C). The use of Total Green Area was a more
242 standardized parameter since it was less susceptible to variability compared to the Total Green
243 Intensity parameter (e.g. led intensity, exposure time, and dye concentration). In addition to
244 delineating cytotoxic and cytostatic therapy responses, our platform allowed for kinetic monitoring
245 of therapy-induced cell death (Fig. 6D) and assessment of organoid health (growth and viability)
246 as an imperative run quality control (Fig. 6E). Moreover, our platform allowed for more in-depth

247 research on the type of therapy-induced cell death that occurred. For example, cisplatin induced
 248 caspase 3/7 activity in NSCLC_046T, which is partly inhibited by the pan-caspase inhibitor Z-
 249 VAD-FMK (Fig. 6F). Consistently, Z-VAD-FMK inhibited cisplatin induced cell death, indicating
 250 that cytotoxicity occurs through caspase-dependent apoptosis (Fig. 6G). Here, the importance of
 251 kinetic monitoring is further highlighted, as the inhibitory effect of Z-VAD-FMK is nullified at
 252 72h.
 253 Overall, we demonstrated that the OrBITS platform allowed for kinetic and endpoint analysis of
 254 therapy-induced cell death to distinguish cytostatic from cytotoxic responses and can be further
 255 developed to provide in-depth insight into the mechanistic action.



256
 257 **Figure 6: Fluorescent/brightfield imaging as a cell death marker.** (A) Pairwise comparison of Total Green
 258 Intensity and Total Green Area (Cytotox Green reagent) normalized to Total BF Area with the luminescent read-out
 259 (counts/s) of the CellTiter-Glo 3D assay for the NSCLC_051T, NSCLC_051N, co-culture NSCLC_051T/N and
 260 NSCLC_050N PDO lines treated with a 10-point titration of cisplatin (Table S2). (B) Inhibitory (% survival,
 261 normalized to vehicle (100%) and baseline control (0%, 100 μ M cisplatin) and stimulatory (% cell death, normalized
 262 to vehicle (0%) and positive control (100% , 100 μ M cisplatin) dose-response curves and the corresponding IC50 and
 263 EC50 values for NSCLC_051T PDOs treated with a 10-point titration of cisplatin. (C) Inhibitory (% survival,
 264 normalized to vehicle (100%) and baseline control (0%, 1 μ M staurosporine) and stimulatory (% cell death,

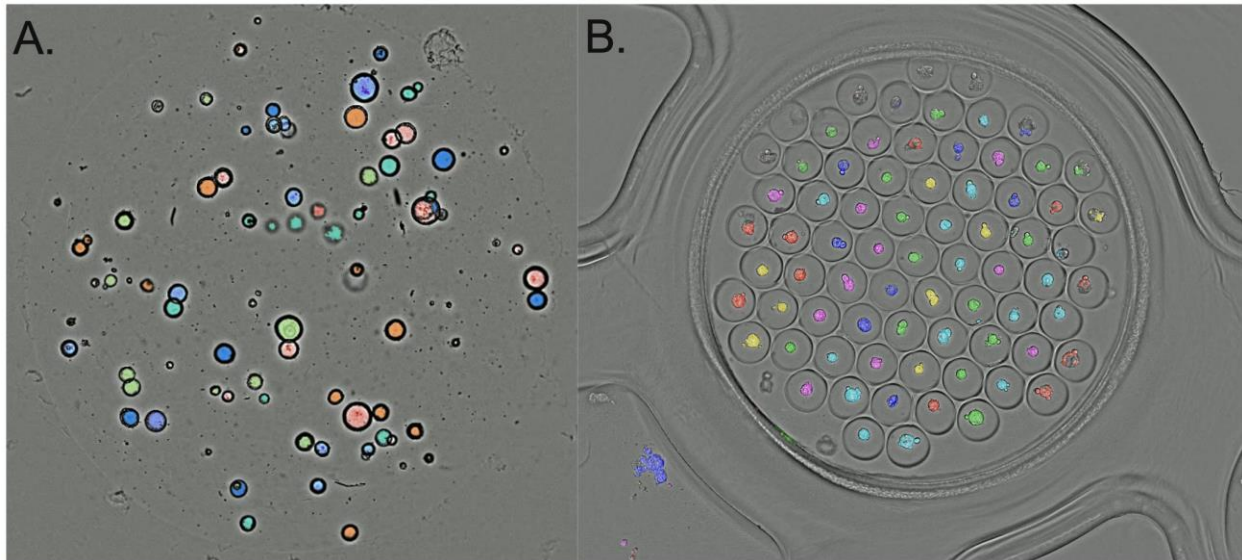
265 normalized to vehicle (0%) and positive control (100% , 1 μ M staurosporine) dose-response curves NSCLC_013T
266 PDOs treated with a 7-point titration of gefitinib. (D) Real-time monitoring of therapy-induced cell death of
267 NSCLC_051T PDOs treated with a 10-point titration of cisplatin. Total Green Area / Total BF Area was normalized
268 to baseline (0%, vehicle at t = 0h) and positive (100%, 100 μ M cisplatin at t = 72h) controls. (E) Real-time monitoring
269 of organoid growth (Total BF Area – Total Green Area) and cell death (Total Green Area / Total BF Area) as run
270 quality control. (F) Total Green Intensity / Total BF Area of the Caspase 3/7 green reagent in NSCLC_046T PDOs
271 treated with cisplatin +/- Z-VAD-FMK (pan-caspase inhibitor). (G) Percentage of cell death of NSCLC_046T
272 organoids treated with cisplatin +/- Z-VAD-FMK. Total Green Area / Total BF Area was normalized to baseline (0%,
273 lowest value) and positive (100%, 75 μ M cisplatin at t = 72h) controls. Graphs presented as mean \pm SD of 5 technical
274 replicates.

275 *Broad applicability of OrBITS for various organoid platforms and cancer cell lines*

276 While the OrBITS platform was developed using lung organoids in a high-throughput 384-well
277 plate format, we have also successfully implemented the image analysis method for a range of
278 cancer cell lines and PDOs of other tumor types. For example, we demonstrated the precise
279 tracking capability on the growth of 3 cell lines (NCI-H1975, HCT-15, and NCI-H460) and
280 pancreatic cancer-derived organoids, using BF imaging (Supplemental Video 4). Furthermore, we
281 showed that OrBITS was able to accurately mask pancreatic cancer organoids embedded in
282 extracellular matrix domes, which further allows monitoring of routine organoid cultures in
283 various culture plates and long-term screening assays (Fig. 7A, Supplemental Video 5). Lastly,
284 OrBITS BF image analysis was tested on the Gri3D[®]-96 well plates, a novel organoid plate format
285 with hydrogel-based microcavities for high-throughput organoid cultures¹⁴. Impressively, OrBITS
286 accurately discriminated organoids from background in the BF images without additional training
287 of the convolutional neural network (Fig. 7B, Supplemental Video 6). Overall, we showed that the
288 OrBITS platform has broad applicability, in terms of various cell and organoid types, as well as
289 culturing methods, ranging from conventional to state-of-the art.

290

291



292
293 **Figure 7: Examples of the broad applicability of OrBITS.** (A) Cystic pancreatic cancer
294 organoids grown in an extracellular matrix dome. Kinetic growth monitoring is shown in
295 supplemental video 5. (B) Cancer cell line spheroids grown in a Gri3D®-96 well plate. Kinetic
296 growth monitoring is shown in supplemental video 6.

297 Discussion

298 In this study we validated a new brightfield imaging-based method for ex vivo drug screening on
299 patient-derived organoids. The Spark Cyto 600 system used here is a state-of-the art multimode
300 plate reader with BF and fluorescence imaging capabilities. With full environmental controls (e.g.
301 O₂, CO₂, temperature) and an injector, we automated the system to plate single cells or full-grown
302 organoids, perform kinetic measurements, and dispense reagents (e.g. CellTiterGlo-3D) for
303 endpoint analysis. This greatly improves the organoid culture by reducing variability involved with
304 the cumbersome manual cultures, particularly in 384-well plates. While this all-in-one system ideal
305 for the clinical implementation of drug sensitivity screens on patient-derived tumor organoids, the
306 current limitation is the Image Analyzer software, which is limited to 2D analysis. Therefore, we
307 developed a deep learning solution for 3D organoid/spheroid segmentation based on BF images

308 acquired with the Spark Cyto. Altogether, these features make up our OrBITS platform which
309 provides, an advanced high-throughput, time-lapse drug screening platform.

310 Our system identifies organoids from BF images, thus removing the need for nuclear labeling,
311 which can affect biological process and confound therapy responses. As demonstrated, there are
312 several benefits to using the BF channel to detect and measure organoids over transient or stably
313 expressed fluorescent markers. These include: (i) the ability to detect organoids in cases where
314 high cell death reduces detectability via nuclear markers; (ii) increased reproducibility since
315 variance related to dye concentrations, stability (e.g. photobleaching), LED intensity, and exposure
316 time is removed; (iii) the ability to detect cystic organoids, which can be problematic since Hoechst
317 only stains the outer edge of cystic organoids; (iv) optimal size and growth metrics, since it is not
318 guaranteed that all parts of the cellular structure will contain viable nucleated cells as organoids
319 grow, and therefore, reliance of fluorescent markers therefore must be limited; (v) the ability to
320 distinguish valid organoids from artifacts such as cellular debris which may produce false positives
321 or bubbles which may occlude cells; (vi) and lastly, the reduction of any interfering effects of
322 repeated fluorescence imaging on growth and metabolism due to the release of reactive oxygen
323 species by photoexcited fluorophores and other side-effects related to phototoxicity¹⁵.

324 Without the need to consider cytotoxic interference, imaging can be performed at higher frequency
325 time intervals. This opens up new possibilities for studies into how drugs affect organoid growth
326 and migration over time, which is currently not possible with simple endpoint assays. A key
327 measurement parameter of drug screening studies is cell viability. This is commonly done using
328 CellTiter-Glo 3D which, as an endpoint assay, is highly constrained. Alternatives to CellTiter-Glo
329 3D for measurement of cell death and viability are especially welcomed, since several therapies

330 are known to affect the primary parameter of measurement for CellTiter-Glo 3D (ATP) via
331 modulating intracellular ATP levels or releasing extracellular ATP following (immunogenic) cell
332 death¹⁶. Furthermore, this approach does not distinguish cytotoxic from cytostatic responses,
333 which could further improve translatability of drug responses to the clinic and requires further
334 investigation.

335 Using the OrBITS platform, we demonstrated that organoid can be grown from either single-cells
336 or full-grown organoids with equal efficiency in 384-well plates. Gao et. al recently demonstrated
337 that organoids starting from single-cells demonstrated similar sensitivity to cytotoxic drugs to
338 matched full grown organoids¹⁷. Therefore, our platform can greatly reduce turn-around time for
339 *ex vivo* drug screenings as OrBITS can accurately monitoring organoid growth, health and therapy
340 response with a limited amount of starting material. In addition, kinetic imaging allows for early
341 detection of therapy response and the use of growth rate metrics has been shown to result in higher
342 reproducibility via uncoupling the effect of cell proliferation on drug sensitivity^{18,19}.

343 Here, we demonstrated organoid identification, growth, and death using BF images, but we have
344 only begun to tap into the potential of BF image analysis. In principle, other morphological
345 changes with clinical and research implications are currently being pursued for organoids, 3D
346 spheroid cultures, and 2D monolayers. We also demonstrated the flexibility of the OrBITS
347 platform to differing culture methods ranging from conventional (e.g. well-plates, matrix domes)
348 to state-of-the-art (Gri3D[®]-96). Furthermore, we demonstrate the analysis capability on various
349 cell and organoids lines apart from those used for developing the BF imaging software. In the
350 process, we confirmed the challenges related to establishing lung cancer organoids as described
351 by Dijkstra et al.¹³. A more minimal medium compared to the one used in this study has recently

352 been described which should limit the growth of normal lung organoids ²², although we observed
353 no sustained organoid growth tested in a small set of samples. The use of Napsin A, p63 or p40
354 (Δ Np63) and TTF-1 allows for identifying cultures overgrown by non-malignant lung cells. As
355 such, the patient-derived organoids used in our method development were non-malignant
356 organoids displaying either a solid (derived from tumor tissue) or cystic (derived from healthy
357 tissue) growth pattern. Apart from the clear difference in morphology, the non-malignant
358 organoids derived from tumor tissue (NSCLC_051T) were more sensitive to cisplatin compared
359 to the organoids derived from healthy tissue from the same patient (NSCLC_051N). This further
360 indicates that these cells have different characteristics which could influence the outcome of a drug
361 sensitivity screen if present in tumor organoid cultures. Even so, our method will also be applicable
362 in tumor organoids since they present a similar growth pattern ^{13,22}.

363

364

365 **Methods**

366 **Patient tissue**

367 Tumor tissue and normal lung tissue (distant from the tumor site) were obtained from adeno- and
368 squamous cell carcinoma NSCLC patients undergoing curative surgery at the Antwerp University
369 Hospital (UZA) in 2019-2020. Written informed consent was obtained from all patients, and the
370 study was approved by the UZA Ethical Committee (ref. 17/30/339). All samples were registered
371 in the Biobank Antwerp, Belgium; ID: BE 71030031000.

372 **Tissue processing and organoid culture**

373 Tissue was stored in Ad-DF+++ (Advanced DMEM/F12 (GIBCO), with 1% GlutaMAX
374 (GIBCO), 1% HEPES (GIBCO), 1% penicillin/streptomycin (GIBCO) supplemented with 2%
375 Primocin (Invivogen) at 4°C and transported on ice to be processed within 24 hours for organoid
376 culture according to the protocol of Dijkstra et al.¹³ with some minor differences. Tumor and
377 normal tissue were minced with two scalpels, collected in 0.1% BSA precoated tubes and washed
378 with PBS. Next, fragments were dissociated with 0.5 mg/mL dispase type II (Sigma-Aldrich), 1.5
379 mg/mL collagenase type II (Sigma-Aldrich), 1:500 Primocin and 10 µM Y-27632 (Cayman
380 Chemicals) in Mg^{2+}/Ca^{2+} PBS (GIBCO) for 60 minutes at 37°C. Digested cells were washed three
381 times with PBS and resuspended in 2/3 Cultrex Type 2 (R&D Systems) and 1/3 Full Lung Ad-
382 DF+++ medium and plated in drops which were allowed to solidify for 30 minutes at 37°C after
383 which they were overlaid with Full Ad-DF+++ medium. Full Ad-DF+++ medium consisted of
384 10% Noggin conditioned medium (HEK293-mNoggin-Fc; kindly provided by Hans Clever,
385 Hubrecht Institute), 10% R-spondin-1 conditioned medium (293T-HA-Rspol-Fc; kindly provided
386 by Calvin Kuo, Stanford University), 1 x B27 supplement (GIBCO), 10 mM nicotinamide (Sigma-

387 Aldrich), 25 ng/mM human recombinant FGF-7 (Peprotech), 100 ng/mL human recombinant
388 FGF-10 (Peprotech), 500 nM A83-01 (Tocris), 1 μ M SB202190 (Cayman Chemicals) and 5 μ M
389 Y-27632 (only used after passaging and thawing). For passaging, organoids were digested to single
390 cells with TrypLE Express (GIBCO). For cryopreservation, 3-day old organoids were harvested
391 with Cultrex Harvesting Solution (R&D Systems) and frozen in Recovery Cell Culture Freezing
392 Medium (GIBCO). Samples were tested for Mycoplasma contamination with the MycoAlert
393 Mycoplasma Detection Kit (LONZA).

394 **Immunohistochemical analysis**

395 Early passage organoids were collected using Cultrex Organoid Harvesting Solution (R&D
396 systems), washed with ice-cold PBS, and fixated in 4% paraformaldehyde for 30 minutes at room
397 temperature. Fixed organoids were transferred to a 4% agarose micro-array mold and paraffin-
398 embedded as described before ²³. Five μ m-thick sections were prepared, deparaffinized and
399 rehydrated prior to staining. Sections were subjected to heat-induced antigen retrieval by
400 incubation in a low pH buffer (Envision Flex TRS low pH (DAKO) for 20 min at 97°C (PT-Link,
401 DAKO). Endogenous peroxidase activity was quenched by incubation in peroxidase blocking
402 buffer (DAKO) for 5 min. Slides were stained manually with mouse anti-TTF1 (clone SPT24,
403 Leica, 1/400, 25') and mouse anti-P40 (clone BC28, Biocare, ready-to-use, 30') primary antibodies
404 followed by an incubation with ENVISION Flex+ Mouse Linker (DAKO, 15') for signal
405 amplification. Mouse anti-NapsinA (clone MRQ-60, Cell Marque, 1/350, 35') staining was
406 performed on a DAKO autostainer Link 48. After that the slides were incubated for 25 min with
407 Envision FLEX/HRP (ready-to-use, DAKO) secondary antibody followed by 10 min incubation
408 with the DAB substrate/chromogen detection system (DAKO). The sections were counterstained

409 for 2 min with hematoxylin (0.1%), dehydrated and mounted with Quick-D Mounting Medium
410 (KlinciPath). Sections were imaged using a Leica DM500 microscope equipped with an ICC50 E
411 camera.

412 **In vitro drug screen**

413 Three days before the start of the experiment, organoids were passaged as single cells using
414 TrypLE and plated in Cultrex drops. Subsequently, organoids were harvested with Cultrex
415 Harvesting Solution, collected in 15 mL tubes coated with 0.1% BSA/PBS, washed with Ad-
416 DF+++ and resuspended in 1 mL Full Ad-DF+++ medium (without Y-27632). Next the number
417 of organoids were counted with the Sceptor 2.0 using a 60 μ M sensor (Merck Millipore).
418 Organoids were then diluted in Full Ad-DF+++ and 5% Cultrex on ice to a concentration that
419 results in 500-2000 organoids/60 μ L. 60 μ L of this solution was plated into a 384-well ultra-low
420 attachment microplate (Corning, #4588) using the Tecan Spark Cyto Injector at a speed of 100
421 μ L/s to avoid bubbles. All tubes and the Spark Cyto Injector were primed with 0.1 % BSA/PBS to
422 avoid sticking of the organoids. Next, the plate was centrifuged (100 rcf, 30 sec, 4°C) and
423 incubated for at least 30 minutes at 37°C.

424 All drugs and fluorescent reagents were added to the plate using the Tecan D300e Digital
425 Dispenser. Cytotox Green (75 nM / well, Sartorius), Caspase 3/7 Green Reagent (2.5 μ M / well,
426 Sartorius), Z-VAD-FMK (50 μ M / well, Bachem AG), Erlotinib, Gefitinib, Osimertinib and
427 Afatinib (Selleckchem) were dissolved in DMSO. Hoechst 33342 (50 nM / well, ThermoFisher),
428 Cisplatin (Tocris) and Carboplatin (Selleckchem) were dissolved in PBS to yield a final
429 concentration of 0.3 Tween-20 required for dispensing with the D300e Dispenser.

430 BF, green and blue fluorescence whole-well images (4x objective) were taken with the Tecan
431 Spark Cyto set at 37°C / 5% CO₂ for kinetic experiments in a humidity cassette. For endpoint
432 measurement of ATP levels, 60 µL CellTiter-Glo 3D reagent (Promega) was injected using the
433 Tecan Spark Cyto Injector to each well, shaken for 5 minutes and measured after 30 minutes
434 incubation with the Tecan Spark Cyto luminescence module.

435 Dose-response curves plotted, and IC₅₀-values were calculated using GraphPad Prism 9. Drug
436 concentrations were transformed to log₁₀ and raw data results were normalized to vehicle (100%)
437 and/or baseline control (0%) (Staurosporin 5 µM or 100 µM cisplatin) for viability assessment,
438 and vice versa for cell death assessment. Curves were fitted using the log (inhibitor/agonist) vs.
439 normalized response - Variable slope function. Screen quality was determined by calculating the
440 Z Factor score using the formula ²⁴:

$$441 \quad 1 - \frac{3 * SD (negative control) + 3 * SD (positive control)}{average (negative control) - average (positive control)}$$

442 **Image-based analysis**

443 Following image acquisition with the Tecan Spark Cyto, BF and fluorescence images were
444 analyzed by the University of Antwerp Service Platform: OrBITS Platform. The analysis output
445 from OrBITS (Table S1) was correlated with the current gold standard assays: Hoechst staining
446 (for organoid tracking), Cytotox Green (for organoid death), and the CellTiter-Glo 3D assay (for
447 drug screening).

448 **Acknowledgements**

449 This work was funded in part by the Flanders Research Foundation, 12S9221N (A.L.),
450 12S9218N (A.L.), G044420N (A.B., S.V., A.L.) and by the Industrial Research Fund of the

451 University of Antwerp, PS ID 45151 (C.D., S.V., A.L.). We would like to thank Mr. Willy
452 Floren for funding the D300e and Tecan for gifting the Spark Cyto as part of a competition.

453 **Authors contribution**

454 C.D, E.C.DLH. and A.L. conceived the idea and wrote the manuscript. C.D., M.L.C. performed
455 the in vitro experiments. E.C.DLH. developed the software and analyzed the data. P.V.S., J.M.H,
456 P.L, S.K.Y supplied the patient derived materials. F.L, P.P, A.B, E.S., A.L. substantially revised
457 the manuscript.

458 **Competing interests**

459 The authors declare no competing interests.

460 **References**

- 461 1 Drost, J. & Clevers, H. Organoids in cancer research. *Nat Rev Cancer* **18**, 407-418,
462 doi:10.1038/s41568-018-0007-6 (2018).
- 463 2 Narasimhan, V. *et al.* Medium-throughput Drug Screening of Patient-derived Organoids from
464 Colorectal Peritoneal Metastases to Direct Personalized Therapy. *Clinical cancer research : an*
465 *official journal of the American Association for Cancer Research*, doi:10.1158/1078-0432.CCR-20-
466 0073 (2020).
- 467 3 Ooft, S. N. *et al.* Patient-derived organoids can predict response to chemotherapy in metastatic
468 colorectal cancer patients. *Science translational medicine* **11**, doi:10.1126/scitranslmed.aay2574
469 (2019).
- 470 4 Driehuis, E. *et al.* Pancreatic cancer organoids recapitulate disease and allow personalized drug
471 screening. *Proceedings of the National Academy of Sciences of the United States of America*,
472 doi:10.1073/pnas.1911273116 (2019).
- 473 5 Driehuis, E. *et al.* Patient-Derived Head and Neck Cancer Organoids Recapitulate EGFR Expression
474 Levels of Respective Tissues and Are Responsive to EGFR-Targeted Photodynamic Therapy. *J Clin*
475 *Med* **8**, doi:10.3390/jcm8111880 (2019).
- 476 6 Driehuis, E. *et al.* Oral Mucosal Organoids as a Potential Platform for Personalized Cancer Therapy.
477 *Cancer discovery* **9**, 852-871, doi:10.1158/2159-8290.Cd-18-1522 (2019).
- 478 7 Vlachogiannis, G. *et al.* Patient-derived organoids model treatment response of metastatic
479 gastrointestinal cancers. *Science* **359**, 920-926, doi:10.1126/science.aao2774 (2018).
- 480 8 Nagle, P. W., Plukker, J. T. M., Muijs, C. T., van Luijk, P. & Coppes, R. P. Patient-derived tumor
481 organoids for prediction of cancer treatment response. *Seminars in cancer biology* **53**, 258-264,
482 doi:10.1016/j.semcancer.2018.06.005 (2018).
- 483 9 Choi, Y. M. *et al.* Mechanism of Cisplatin-Induced Cytotoxicity Is Correlated to Impaired
484 Metabolism Due to Mitochondrial ROS Generation. *PLoS one* **10**, e0135083,
485 doi:10.1371/journal.pone.0135083 (2015).

- 486 10 Shirmanova, M. V. *et al.* Chemotherapy with cisplatin: insights into intracellular pH and metabolic
487 landscape of cancer cells in vitro and in vivo. *Sci Rep* **7**, 8911, doi:10.1038/s41598-017-09426-4
488 (2017).
- 489 11 Zhou, Y. *et al.* Intracellular ATP levels are a pivotal determinant of chemoresistance in colon cancer
490 cells. *Cancer research* **72**, 304-314, doi:10.1158/0008-5472.Can-11-1674 (2012).
- 491 12 Turner, B. M. *et al.* Napsin A, a new marker for lung adenocarcinoma, is complementary and more
492 sensitive and specific than thyroid transcription factor 1 in the differential diagnosis of primary
493 pulmonary carcinoma: evaluation of 1674 cases by tissue microarray. *Arch Pathol Lab Med* **136**,
494 163-171, doi:10.5858/arpa.2011-0320-OA (2012).
- 495 13 Dijkstra, K. K. *et al.* Challenges in Establishing Pure Lung Cancer Organoids Limit Their Utility for
496 Personalized Medicine. *Cell Rep* **31**, 107588, doi:10.1016/j.celrep.2020.107588 (2020).
- 497 14 Brandenberg, N. *et al.* High-throughput automated organoid culture via stem-cell aggregation in
498 microcavity arrays. *Nat Biomed Eng* **4**, 863-874, doi:10.1038/s41551-020-0565-2 (2020).
- 499 15 Icha, J., Weber, M., Waters, J. C. & Norden, C. Phototoxicity in live fluorescence microscopy, and
500 how to avoid it. *Bioessays* **39**, doi:10.1002/bies.201700003 (2017).
- 501 16 Krysko, D. V. *et al.* Immunogenic cell death and DAMPs in cancer therapy. *Nat Rev Cancer* **12**, 860-
502 875, doi:10.1038/nrc3380 (2012).
- 503 17 Gao, M. *et al.* Development of a Single-Cell Technique to Increase Yield and Use of Gastrointestinal
504 Cancer Organoids for Personalized Medicine Application. *J Am Coll Surg*,
505 doi:10.1016/j.jamcollsurg.2020.11.009 (2020).
- 506 18 Driehuis, E., Kretzschmar, K. & Clevers, H. Establishment of patient-derived cancer organoids for
507 drug-screening applications. *Nat Protoc* **15**, 3380-3409, doi:10.1038/s41596-020-0379-4 (2020).
- 508 19 Hafner, M., Niepel, M., Chung, M. & Sorger, P. K. Growth rate inhibition metrics correct for
509 confounders in measuring sensitivity to cancer drugs. *Nat Methods* **13**, 521-527,
510 doi:10.1038/nmeth.3853 (2016).
- 511 20 Baker, L. A., Tiriach, H. & Tuveson, D. A. Generation and Culture of Human Pancreatic Ductal
512 Adenocarcinoma Organoids from Resected Tumor Specimens. *Methods in molecular biology*
513 **1882**, 97-115, doi:10.1007/978-1-4939-8879-2_9 (2019).
- 514 21 Kassis, T., Hernandez-Gordillo, V., Langer, R. & Griffith, L. G. OrgaQuant: Human Intestinal
515 Organoid Localization and Quantification Using Deep Convolutional Neural Networks. *Sci Rep* **9**,
516 12479, doi:10.1038/s41598-019-48874-y (2019).
- 517 22 Kim, M. *et al.* Patient-derived lung cancer organoids as in vitro cancer models for therapeutic
518 screening. *Nature communications* **10**, 3991, doi:10.1038/s41467-019-11867-6 (2019).
- 519 23 Ivanov, D. P. & Grabowska, A. M. Spheroid arrays for high-throughput single-cell analysis of spatial
520 patterns and biomarker expression in 3D. *Sci Rep* **7**, 41160, doi:10.1038/srep41160 (2017).
- 521 24 Zhang, J. H., Chung, T. D. & Oldenburg, K. R. A Simple Statistical Parameter for Use in Evaluation
522 and Validation of High Throughput Screening Assays. *J Biomol Screen* **4**, 67-73,
523 doi:10.1177/108705719900400206 (1999).

524